CHEMISTRY OF MATERIALS
Cite This: Chem. Mater. 2019, 31, 6076−6083
Article
pubs.acs.org/cm

Evidence for Strong and Weak Phenyl-C_{61}-Butyric Acid Methyl Ester Photodimer Populations in Organic Solar Cells

Sebastian Pont,[†,‡] Silvio Osella,[§] Alastair Smith,[‡] Adam V. Marsh,[†,‡] Zhe Li,[∥] David Beljonne,[⊥] João T. Cabral,*[,†,#] and James R. Durrant*[,†,‡,▽]

[†]Centre for Plastic Electronics, Imperial College London, London SW7 2AZ, United Kingdom
[‡]Department of Chemistry, Imperial College London, London SW7 2AZ, United Kingdom
[§]Chemical and Biological Systems Simulation Lab, Center of New Technologies, University of Warsaw, Banacha 2C, 02-097 Warsaw, Poland
[∥]School of Engineering, Cardiff University, Cardiff CF24 3AA, United Kingdom
[⊥]Center for Research in Molecular Electronics and Photonics, University of Mons, 7000 Mons, Belgium
[#]Department of Chemical Engineering, Imperial College London, London SW7 2AZ, United Kingdom
[▽]College of Engineering, Swansea University, Bay Campus, Swansea SA1 8EN, United Kingdom

Supporting Information

ABSTRACT: In polymer/fullerene organic solar cells, the photochemical dimerization of phenyl-C_{61}-butyric acid methyl ester (PCBM) was reported to have either a beneficial or a detrimental effect on device performance and stability. In this work, we investigate the behavior of such dimers by measuring the temperature dependence of the kinetics of PCBM de-dimerization as a function of prior light intensity and duration. Our data reveal the presence of both "weakly" and "strongly" bound dimers, with higher light intensities preferentially generating the latter. DFT simulations corroborate our experimental findings and suggest a distribution of dimer binding energies, correlated with the orientation of the fullerene tail with respect to the dimer bonds on the cage. These results provide a framework to rationalize the double-edged effects of PCBM dimerization on the stability of organic solar cells.

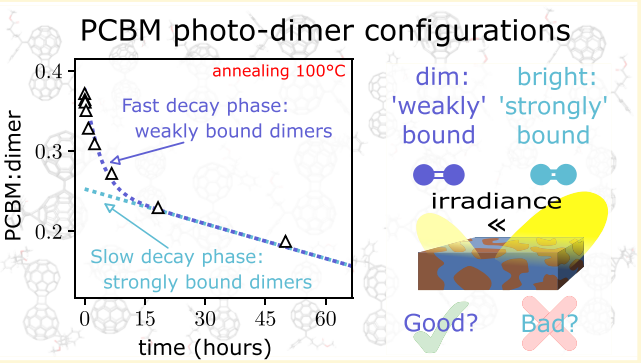

1. INTRODUCTION

To realize the growing potential of organic solar cells (OSCs), improvements in operational stability remains a key challenge.[1] The development of new polymers and acceptors is continuing to increase the efficiency of OSCs.[2−4] The current record certified power conversion efficiency is over 17%,[5] achieved in a tandem device architecture incorporating fullerene and nonfullerene electron acceptors. However, the potential loss of OSC power conversion efficiency over time is a key concern for commercialization. This loss can be caused by various stress factors. Environmental elements such oxygen and humidity can react with materials within the device; these factors may be encapsulated against in certain applications, such as those employing glass encapsulation. However, intrinsic factors such as thermal stress, illumination, and interlayer stability cannot be encapsulated against and therefore are always present during operation.[6−8] In particular, OSCs are often observed to undergo significant light induced degradation during the initial stages of operation. This is termed the "burn-in" and is related to several loss mechanisms which are current areas of interest.[9−11] Other studies have highlighted the potential for thermally induced degradation of performance, often associated with changes in film morphology.[12−14] The light induced dimerization of the most widely used, fullerene-based, electron acceptor PCBM (phenyl-C_{61}-butyric acid methyl ester) was reported to be a factor in both of these intrinsic degradation pathways, in some cases detrimentally[15,16] as the underlying cause of device "burn-in", and in other cases beneficially[17−19] in improving film morphological stability. In this study, we focus on these apparently contradictory effects of PCBM dimerization and, in particular, provide evidence that light irradiation can result in the formation of two distinct populations of PCBM dimers depending upon the irradiation conditions used (Figure 1).

The dimerization of fullerenes in OSC bulk heterojunctions is known to occur during operating conditions.[15−17] Beneficial

Received: December 17, 2018
Revised: May 2, 2019
Published: May 3, 2019

DOI: 10.1021/acs.chemmater.8b05194
Chem. Mater. 2019, 31, 6076−6083

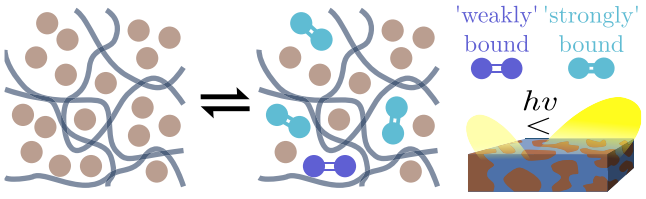

Figure 1. Upon illumination PCBM undergoes a 2 + 2 cycloaddition reaction to form dimers. These are thermally reversible at elevated temperatures. In polymer:fullerene bulk heterojunctions distinct dimer populations are found to occur that have varying stability to de-dimerization. This is associated with the configuration of the asymmetric PCBM units in the dimers. At high light irradiances predominately "strong" dimers are formed, whereas at lower light intensities "weak" PCBM dimers are formed. These results present a pathway to understand the simultaneous beneficial and detrimental effects of PCBM dimerization in OSCs.

effects of PCBM dimerization have been correlated with improved morphology stability in a number of polymer:-fullerene systems.[17−19] PCBM crystallization and aggregation is one of the key causes of morphological degradation under thermal stress; the formation of the PCBM dimers unit was suggested to impede the nucleation of such PCBM crystallites, thereby enhancing film and device stability.[17] The dimer is also immobile compared to the monomer unit.[19] However, neutral effects of PCBM dimerization have been observed by Inasaridze et al. within systems of no burn-in despite dimerization occurring and systems with burn-in without dimerization occurring.[20] Furthermore, other reports have suggested detrimental effects of PCBM dimerization on the performance and stability of OSCs. Distler et al. reported that dimerization was correlated with the formation of trap states during the degradation of PDTSTzTz:PCBM devices.[15] More recently, Heumueller et al. presented further examples of PCBM dimerization causing device degradation in seven different polymer:fullerene material systems.[16] From these results, it is clear the effect of fullerene dimerization on stability is nontrivial and the current models in the literature present conflicting conclusions.

The first study of the photochemical dimerization of C_{60} was reported 20 years ago by Rao et al.[21] This 2 + 2 cycloaddition reaction was proposed to be driven by photogenerated fullerene triplet states.[22] The dimerization was observed in other fullerenes, such as C_{70} and PCBM, but at slower rates of formation, attributed to asymmetry and steric hindrance effects.[23,24] The topological criteria for dimerization is the alignment of two carbon−carbon double bonds at a separation of less than 4.2 Å. In crystalline PCBM, this requirement is met, with a fullerene cage separation of 3.5 Å. Conversely, PCBM crystallization was reported to lower the yield of long-lived triplet states.[25] Temperature dependence studies on C_{60} show it freely rotates about its center of mass at and above room temperature.[26] Although there are many criteria for dimerization, the 30 × 30 = 900 possible orientations have been suggested to aid with the relatively high yields of dimerization in neat C_{60} films.[27] For C_{60}, thermally induced de-dimerization was observed, with an activation energy of 1.25 eV.[26] The de-dimerization in $PC_{60}BM$ dimers was studied by Wong et al.[18] The reaction kinetics are found to be very similar to those of C_{60}, with an activation energy of 0.96 eV.

To study the kinetics of PCBM dimerization an absorbance assay was used to probe the fraction of dimers to monomers.[15,16,28] This facile assay enables time-resolved monitoring of the PCBM dimerization and de-dimerization. A representative bulk heterojunction of PCDTBT:PCBM thin films was exposed to varying duration and intensity of light exposure followed by dark thermal annealing. By analyzing the kinetics of the thermal de-dimerization, the resulting PCBM dimer enthalpy of dissociation (referred to herein as the dimer binding energy) are correlated with light intensity and duration. This work presents a framework to understand the conflicting effects of PCBM dimerization in OSCs and strategies to maximize both performance and stability.

2. EXPERIMENTAL SECTION

Sample Preparation. Solutions of phenyl-C61-butyric acid methyl ester, PCBM, supplied by Nano-c and poly[*N*-9′-heptadecanyl-2,7-carbazole-*alt*-5,5-(4′,7′-di-2-thienyl-2′,1′,3′-benzothiadiazole)], PCDTBT, supplied by 1-materials were prepared at a combined concentration of 25 mg mL^{-1} in chlorobenzene. Glass substrates were plasma treated in an oxygen atmosphere with an Emitech K1050X before solutions of 1:2 PCDTBT:PCBM were spin coated at 1500 rpm for 30 s. The resulting film thicknesses were ≈100 nm, measured by stylus profilometry (Dektak XT). For the GPC measurements the samples were redissolved in chlorobenzene.

Illumination and Annealing. Illumination and annealing were carried out in a nitrogen filled glovebox with oxygen and humidity levels kept < 15 ppm. A Bridgelux 4000 K white LED light source was used with the spectrum previously reported.[19] For thermal stress, temperatures were controlled with a hot plate or cooling plates and calibrated with an IR temperature sensor in the presence of the illumination to ensure accurate temperature control.

UV−Visible Absorption Spectroscopy. UV−visible absorption spectroscopy was carried out with a Shimadzu UV-1601 spectrophotometer. Measurements were taken from 300 to 350 nm in transmission mode. To determine an assay of PCBM dimer concentration the absorbance was normalized to a peak at ≈340 nm, and the change at the peak minimum at ≈320 nm was monitored.

Density Functional Theory (DFT) Simulations. DFT simulations were optimized with the B3LYP functional and the 6-31G(d) Pople's basis set. To study all possible dimer conformations and to take into account the symmetry of the system, two steps have been considered. In the first, one bond was considered fixed and one by one all the possible dimers with the other PCBM were created. Next, considering the most stable sites obtained from the first step, new dimers have been created and conformations analyzed. Since it is not possible to computationally study all 689 possible configurations, only selected ones have been considered, for a total of 49 dimers. To calculate the aromaticity of the rings forming PCBM before and after the dimer formations, the NICS indexes have been considered. A single point energy calculation was performed on the selected PCBM and position 8 considering the center of all rings (NICS(0)) and at the center of the PCBM sphere.

Gel Permeation Chromatography. Gel permeation chromatography with in situ optical measurements was performed using an Agilent Technologies 1260 Infinity GPC System with 1260 RID and DAD VL attachments. Measurements were performed at 80 °C, using analytical grade chlorobenzene as eluent with two PLgel 10 μm MIXED B columns in series. Samples were prepared using analytical grade chlorobenzene in concentrations of 1 mg mL^{-1} to 2 mg mL^{-1} and filtered with VWR PES membrane 0.45 μm syringe filters before submission. An injection volume of 50 μL and GPC flow rate of 1.00 mL min^{-1} was used. The absorbances at 300, 320, and 335 nm were used to monitor the elution and found to give equivalent results.

3. RESULTS AND DISCUSSION

3.1. Distinct Dimer Populations. In this study, the kinetics of thermally induced PCBM de-dimerization are probed in polymer:fullerene blends in order to investigate the

DOI: 10.1021/acs.chemmater.8b05194
Chem. Mater. 2019, 31, 6076−6083

energetic distribution of dimer binding strengths. Previous studies have probed the yields of de-dimerization using gel permeation chromatography (GPC) or high-performance liquid chromatography (HPLC).[15,16,18] Time-resolved measurements with these techniques are impractical as they require destruction of the sample and are time intensive to perform. Recently, it was shown that the relative proportions of PCBM monomer and dimer states can be readily assayed from UV/visible absorption spectroscopy.[15,19] This absorbance assay facilitates collecting time-resolved dimer concentrations, enabling analysis of the kinetics of PCBM dimerization and de-dimerization, as detailed below.

To investigate the de-dimerization kinetics, PCDTBT:PCBM films were initially irradiated with a white light LED (with negligible UV light, see Figure S1 for spectrum) to induce partial PCBM dimerization, and then annealed at 100 °C in the dark to induce de-dimerization. Absorbance spectra were taken periodically while annealing to monitor the kinetics of de-dimerization. Specifically, the change in an absorbance feature at 320 nm was converted to a dimer:monomer ratio using a calibration shown in Figure S2 and reported in more detail elsewhere.[28] In short, polymer:PCBM films were exposed to a range of irradiances and radiant exposures, and the resulting change in absorbance was calibrated against absolute dimer concentration determined from gel permeation chromatography data. Figure 2 presents

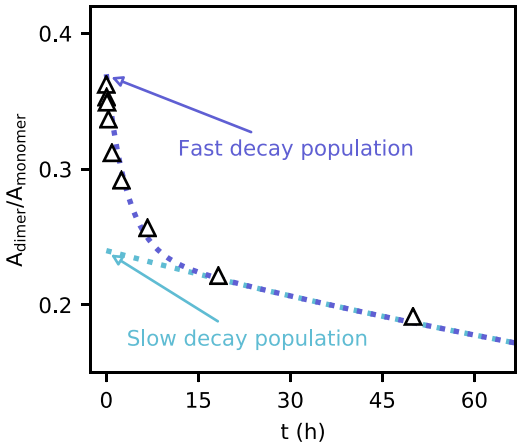

Figure 2. PCBM dimer:monomer ratio of a 1:2 PCDTBT:PCBM thin film while annealing at 100 °C in the dark. The film had prior illumination at 186 W m^{-2} for 82 h which resulted in the PCBM dimer concentration at t = 0 min. Two phases of de-dimerization are observed: first, a fast-phase with rate of ≈181 min^{-1} upon which the "weakly" bound dimers separate and, second, a slow-phase with a rate of ≈12.6 × 10^3 min^{-1} where "strongly" bound dimers separate.

dimer population decay over time following prior irradiation at 186 W m^{-2} for 82 h. Complete reversibility of the photodimerization has previously been shown to occur in this system and is therefore expected to occur here at very long time scales.[18,26] It was expected that the decay would follow the reaction model described by Eklund and co-workers and used in previous analyses of the de-dimerization kinetics.[26] This model states the dimer concentration, D, should exhibit a (monoexponential) decay over time upon isothermal annealing, following where $D(t) = D(t_0)\exp(-kt)$ at time t and decay rate k. Using this model, Eklund and co-workers were able to precisely fit the thermal transformation of polymeric C_{60} to monomeric C_{60} showing the validity of this model for C_{60}.[22,26]

However, a monoexponential decay does not fit the data in Figure 2. Empirically, we find that a bi-exponential decay describes all data in full:

$$D(t) = D_{slow}\exp(-k_{slow}t) + D_{fast}\exp(-k_{fast}t) \quad (1)$$

where D is dimer concentration at time t, D_{slow} and D_{fast} are termed the slow and fast phases, respectively, and k_{slow} and k_{fast} are the associated decay rate constants, respectively. The bi-exponential trend is also clearly observed in polystyrene:PCBM films as shown in Figure S3. Several possible interpretations can be considered for this behavior. Fullerenes have been shown to oligomerize,[21] and the formation of PCBM trimers was reported by several groups;[18,21] these could contribute to an additional time decay profile. Alternatively, the dimerization process itself could be nonexponential (e.g., described by a stretched exponential) potentially associated with matrix rearrangements required for thermal decomposition to occur; however, we find that a bi-exponential description provides good agreement with experiment (Figure S4). Given that the light spectrum has a broad frequency range, one could conceivably access different reactions and thus dimer pathways depending on incident photon energy; however, no wavelength dependence in dimerization was reported in PCBM films.[24] Finally, we hypothesize that the intrinsic distribution of relative spatial configurations of PCBM molecules with a film might result in the formation of distinct photodimers, which could then be expected to exhibit different de-dimerization energetic requirements and thus kinetics. Some evidence for dimer complexity is suggested by structured HPLC traces upon light exposure and redissolution.[16] Next, we experimentally investigate the role of light intensity and time (and thus radiant exposure, or dose) on the de-dimerization time profile to examine this bi-exponential behavior and then report on a theoretical examination of dimer topology.

3.2. Reaction Kinetics of Fast and Slow Decays. The factors determining the ratio of fast to slow phase were investigated by controlling the dimerization illumination conditions prior to annealing. Specifically, three parameters are investigated: the radiant exposure (total energy dose), the irradiance (light intensity), and the duration of the light exposure. First, to probe the effect of radiant exposure, PCDTBT:PCBM films were exposed to a constant 15 kJ m^{-2} from a white light LED array while the irradiance was varied from 63 W m^{-2} to 2155 W m^{-2}. Second, to probe the effect of irradiance, films were illuminated for 50 h with irradiances of 63 W m^{-2} to 2155 W m^{-2}. Lastly, to probe the time dependence, films were exposed to 630 W m^{-2} with a duration of 18 to 14400 min. After, light soaking films were annealed at 100 °C in the dark and absorbance measurements taken intermittently to monitor the de-dimerization. The results of these three conditions are presented in Figure 3a–c. The decay of the dimer population was fitted with eq 1. After fitting with the least-squares error, k_{slow} = 0.135(23) × 10^{-5} s^{-1} and k_{fast} = 9.31(99) × 10^{-5} s^{-1} to one standard deviation for all the decays in Figure 3a–c. As such, we can conclude that the dissociation kinetics of the two separate dimer populations are independent of light irradiation conditions, with differences in overall decay kinetics as a function of light irradiation conditions resulting only from variations in the relative magnitudes of the fast and slow de-dimerization phases.

The previously reported rate of de-dimerization in PCDTBT:PCBM was 2.28 × 10^{-5} s^{-1} which is between the values of the slow and fast kinetics observed here.[18] The

DOI: 10.1021/acs.chemmater.8b05194
Chem. Mater. 2019, 31, 6076–6083

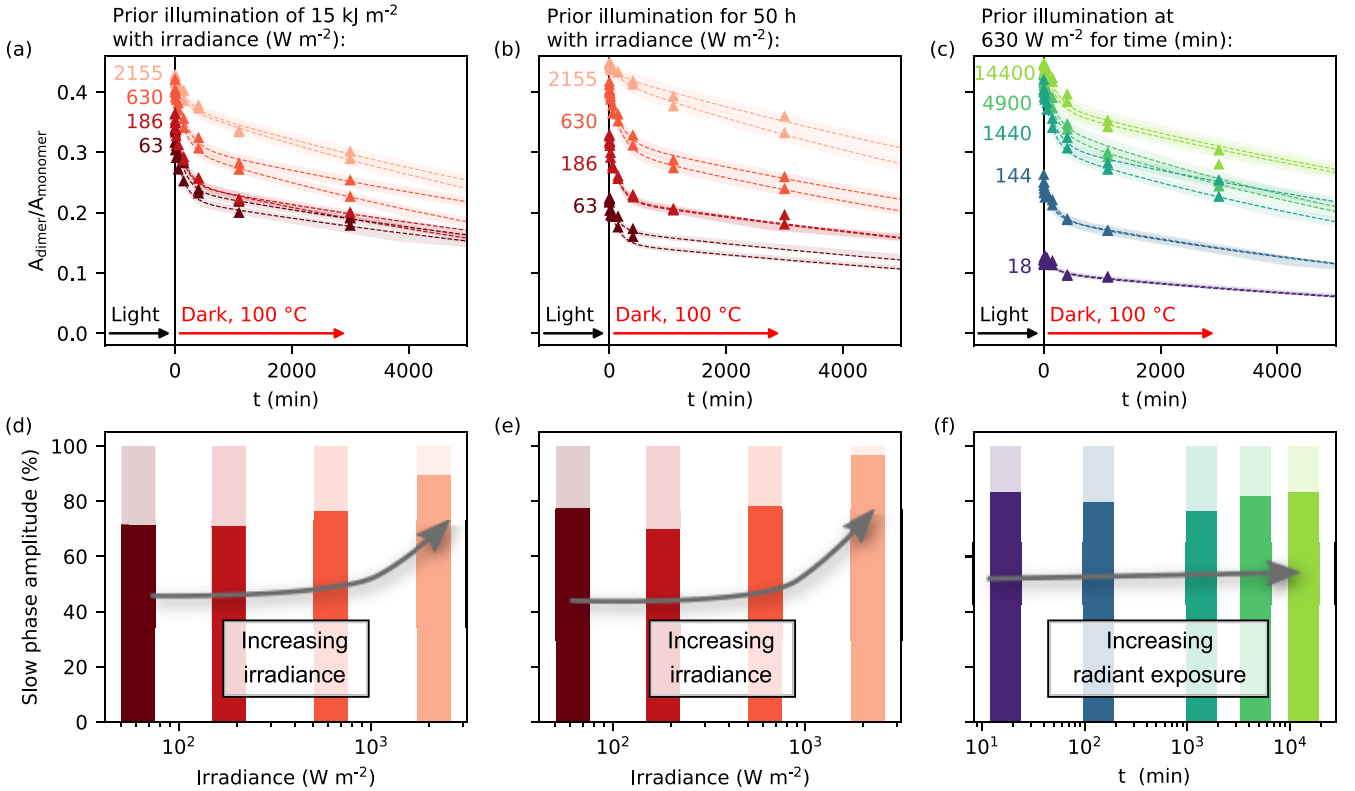

Figure 3. (a–c) PCBM dimer:monomer ratio in PCDTBT:PCBM thin films while annealing at 100 °C in the dark with prior illumination with three scenarios: (a) equal radiant exposure, (b) equal illumination time, and (c) equal irradiance. For each measurement repeats are presented as separate markers. Fitting of the two-phase decay gives the amplitudes of the fast phase and the slow phase after the illumination. (d–f) The percentage of the slow phase formed for the various conditions. These results show the amount of slow phase is dependent on irradiance and not radiant exposure or illumination time.

percentage of slow phase to total dimer ($D_{slow}/[D_{slow} + D_{fast}]$) is plotted in Figure 3d–f. Figure 3d,e broadly presents the trend that illumination at a higher irradiance causes a greater fraction of slow phase, independent of the radiant exposure or duration of light soaking. In Figure 3f, the fraction of the slow phase is independent of illumination duration. The fraction of the fast to slow phase is therefore dependent on the irradiance of illumination and not the duration of illumination or the radiant exposure. From these measurements, it can be concluded that a key factor controlling the distinct populations is the irradiance. Its underlying mechanism was investigated by analyzing the absolute yield of the slow and fast phases. The amplitude of each decay phase (as calculated from Figure 3) was compared with the light duration and with the radiant exposure. Figure 4a shows that the slow phase correlates with the radiant exposure. This follows the expected trend whereby increasing the illumination duration increases the yield of dimers, independent of intensity. However, the fast-phase correlates, within experimental error, with the duration of light exposure (Figure 4b) to a greater extent than to a correlation with radiant exposure (Figure S5a). This is understood as even at the lowest irradiance investigated (63 W m^{-2}) the illumination is not limiting the formation of the fast phase. Therefore, increasing the irradiance does not increase the rate of formation, contrary to the slow-phase amplitude. Instead, for the fast-phase amplitude, there is time dependence limiting the reaction.

3.3. PCBM Trimers. PCBM trimers are examined as the potential cause of one of the fast and slow phases, alongside dimers, observed in the thermal decomposition process. GPC measurements were used to probe the kinetics of PCBM trimer formation. Fullerene light exposure can result in high order units such as trimers and oligomers which will affect the binding energy. In C_{60}, the oligomerization can result in molecules with 21 units.[21] To determine if this mechanism is responsible for the two-phase kinetics of thermal decomposition observed, the illumination dependence on oligomerization of PCBM is investigated. Gel permeation chromatography (GPC) eludes the trimer unit faster than the smaller dimer unit (Figure 5). As with the previous absorbance experiments, a select range of radiant exposure and irradiances were used to determine the reaction kinetics of trimerization. In Figure 5, the trimer signal correlates with radiant exposure (H_e) and is independent of irradiance. This does not follow the trends observed for the formation of the two-phase kinetics where a dependence on irradiance is observed. Furthermore, the fraction of trimer:dimer is determined from the amplitude of each signal in the GPC. The fraction of PCBM trimer to dimer (1:12) does not correlate with the fraction of fast to slow phase (1:4), accounting for reaction stoichiometry. From these observations, it is concluded that PCBM trimerization does not account for the biphase kinetics of decomposition.

3.4. PCBM Dimer Configurations. Another potential mechanism resulting in the formation of populations of dimers with different binding energies is the configuration of the PCBM dimer bond. In C_{60} fullerenes, trimers can form as linear or angled isomers due to variation in bonding location on the cage.[27,29] Therefore, it is likely the PCBM dimerization will occur at a variety of bonding locations. The position of the PCBM tail on each of the fullerene units relative to the dimer

DOI: 10.1021/acs.chemmater.8b05194
Chem. Mater. 2019, 31, 6076–6083

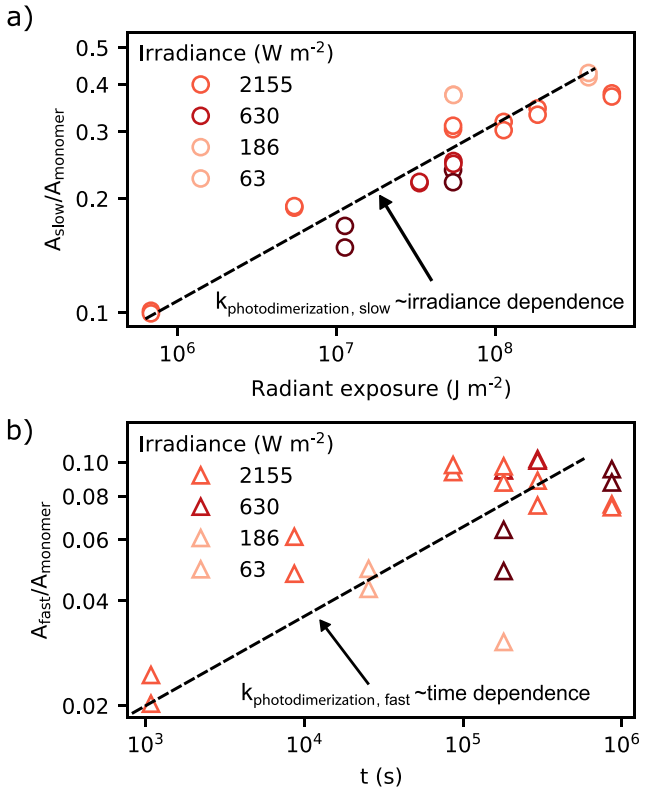

Figure 4. (a) Fraction of the slow decay to total dimerization correlated against prior radiant exposure. This suggests the reaction follows the expected triplet mechanism previously reported for PCBM dimerization. (b) Fraction of the fast decay to total dimerization correlated against prior illumination exposure time. This suggests that even at the lowest irradiance used (63 W m^{-2}) the rate of formation is not limited by the illumination.

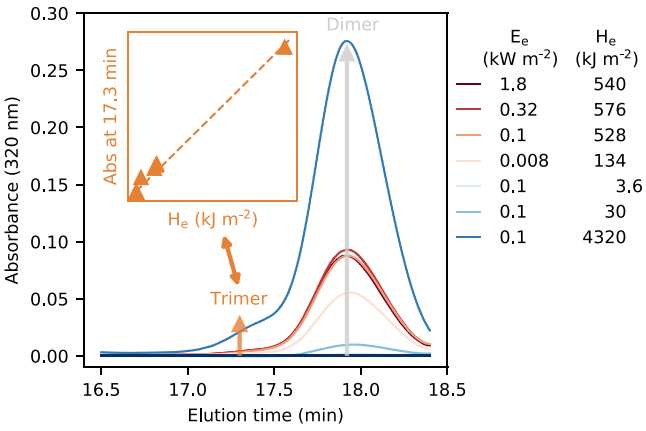

Figure 5. GPC measurements of PCDTBT:PCBM films after varied radiant exposure and irradiance. PCBM trimers are observed in PCDTBT:PCBM films which are identified by a shoulder at 17.3 min in the GPC measurements. The inset shows the linear correlation of trimerization with radiant exposure, H_e. The red traces have similar radiant exposure (≈550 kJ m^{-2}) with irradiances from 0.1 kW m^{-2} to 1.8 kW m^{-2} and all form approximately the same concentration of dimer; therefore, the trimer formation is independent of the irradiance, E_e. This is different to the trend observed between the strong and the weak dimer (E_e dependence); thus, the different dimers are not dimer and trimer formation.

bond location will affect the binding strength. There are 30 double bonds on a C_{60} cage located at the edge of hexagonal faces of a truncated icosahedron and as such called [6,6] double bonds.[21] Aside from the [6,6] double bonds, there are bonds located between a hexagon and pentagon known as [6,5] bonds. These bonds can undergo the 2 + 2 cycloaddition reaction to form fullerene dimers. In C_{60}, a dimer between [6,6]/[6,6] bonds is more stable than the [6,6]/[6,5] bonds or [6,5]/[6,5] bonds by 83 kJ mol^{-1} and 163 kJ mol^{-1}, respectively.[29] Herein, the [6,6] bonds are assumed to be the location of the [2 + 2] cycloaddition in PCBM. The symmetry of C_{60} means there is no effect of the dimer bond location on the binding energy, consistent with the monoexponential de-dimerization kinetics reported previously for C_{60}.[22,26] However, due to the asymmetry of PCBM, the location of the dimer bond relative to the PCBM tail will likely affect the associated binding energy. To investigate how significant this effect is density functional theory (DFT) calculations were done on a selection of dimer configurations. On PCBM there are 29 dimer bond locations, excluding the bond with the PCBM tail, resulting in 29 × 29 = 841 possible dimer orientations. The asymmetry of the side group means bonds on each configuration will result in different properties.

To effectively investigate the energetic landscape of the possible 841 PCBM dimer configurations a two-step methodology was used. First, the possible bonding sites were split into 8 classes relating to the distance to the PCBM tail, termed β, as depicted in Figure 6a and Figure S6. Prescreening eliminated the class closest to the PCBM tail (β = 1) leaving 25 possible bond locations. For the first step of calculations, the lone bond at class eight was fixed for fullerene-b (β_b = 8), and this was connected with all 25 bond locations on fullerene-a. All DFT simulations are presented in Figure 6b as an individual ring where the size and color relates to the energy of the binding. From these results, β = 2 and β = 3 dimer binding energies are approximately 100 meV higher than the $\beta \geq 4$ configurations, giving a total distribution of 200 meV for $2 \leq \beta \leq 8$. The variation in binding energy should result in a change of reaction constant as defined by an Arrhenius relationship. The pre-exponenetial factor of the Arrhenius relationship is thought to relate to the collision frequency of bond locations and is, therefore, assumed to be independent of dimer bonding location. In the instance where ΔE_{a-b} = 0.2 eV and assuming the equivalent pre-exponential factor, then k_a:k_b = 504 at 100 °C. Under these conditions, the reaction would be either too slow or too quick and, therefore, β = 2 and β = 3 are assumed to be too unstable and unfeasible. In the instance where ΔE_{a-b} = 0.13 eV as with $\beta \geq 4$, then k_a:k_b= 57.1 at 100 °C. This is remarkably close to the ratio found when modeling the results in Figure 3, where k_{slow}:k_{fast} = 68.6 at 100 °C. Therefore, the configurations of PCBM dimers with β = 2 and β = 3 are energetically unfavorable and thus expected not to form under these conditions. However, energy distribution for dimer configurations at $\beta \geq 4$ are consistent with energies observed experimentally.

For the second step of DFT calculations the remaining configurations with the class of $\beta \geq 4$ are considered. For each class (except β = 8) there are four bonds, meaning a bond between two dimers has 16 possible orientations (i.e., for a dimer between class 7 on dimer *a* and class 6 on dimer *b* the possible orientations are β_a:β_b = 7_1:6_1, 7_1:6_2, 7_2:6_1, etc.). In each case only one was considered, except for the most stable configuration, β_a:β_b = 4:4, where six orientations were calculated. Bonds not calculated with DFT calculations were extrapolated from the dimers with equivalent classes. A

DOI: 10.1021/acs.chemmater.8b05194
Chem. Mater. 2019, 31, 6076−6083

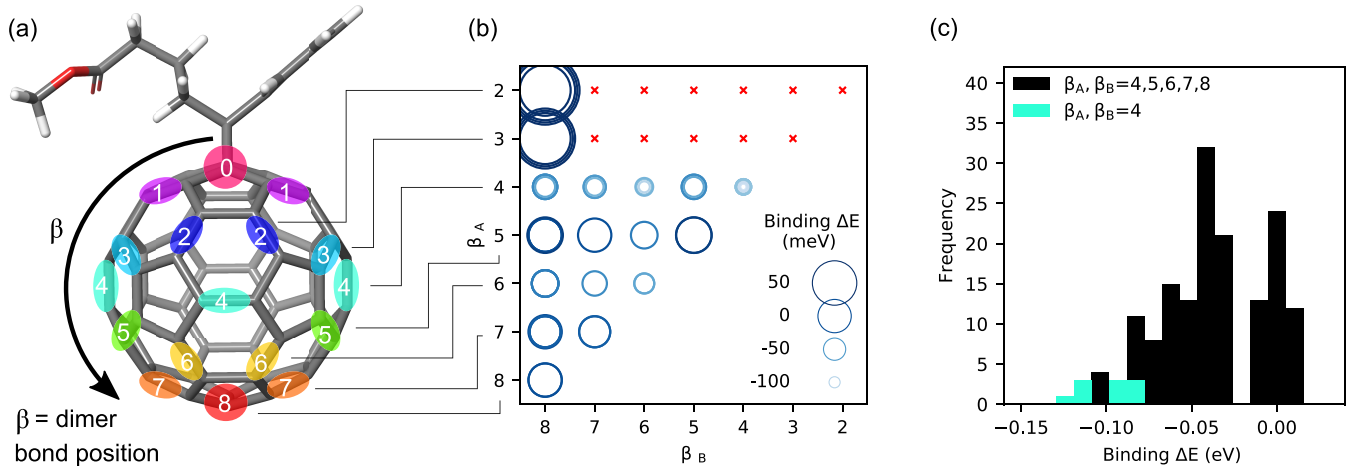

Figure 6. DFT calculations of the possible PCBM dimer configurations. (a) Dimerization sites occur at double bonds between hexagonal faces. There are eight classes of equivalent distance from the PCBM tail unit. (b) PCBM dimer binding energy dependence on the class on each fullerene; namely, β_A and β_B. Each ring represents a different DFT calculation noting that for each β_A:β_B point there are 16 orientations due to the asymmetry of the side group (examples are in Figure S8). Both the size and the color of each ring represent the binding energy relative the β_A:β_B = 8 configuration. (c) Histogram of the binding energies of all possible dimer configurations. The β_A:β_B = 4 dimers are the most stable, and the spread is not as significant compared to the class, β. Thus, the class (β) is a greater factor than the orientation of the PCBM tail of each fullerene.

histogram of all configurations where $\beta \geq 4$ is presented in Figure 6c. The range of energies is >0.1 eV and, therefore, significant within the range of temperatures used in this study.

The correlation between the class, β, and binding energy is considered to understand the origins of the distribution in dimer binding energies. In Figure 6c, bonds at β = 4 and β = 6 are more stable, and specifically β_B:β_A = 4:4 is the most stable. Surprisingly, class eight is not as stable. When dimer bonds are formed with the fullerene cage it distorts the sphere.[30,31] For dimers with the tails parallel to the dimer bond, the width and height of the cage is 7.25 and 7.15 Å, respectively, whereas for dimers with the tails perpendicular to the bond, the width and height of the cage are distorted to 7.00 and 7.47 Å, respectively. If bonds on the fullerene are at opposite sides the distortion will be increased and the strain on the cage will be exaggerated. However, if the bonds are adjacent the distortion and strain are minimized. At bond positions where β = 4 both the steric hindrance of the side chain is minimized and the distortion of the fullerene cage is minimized.

Inspection of the energy landscape for dimer formation suggests that configurations at class β = 4 and 6 yield the lowest energies and that substitutions near the fullerene tail are energetically unfavorable and thus unlikely to occur. We tentatively assign the bi-exponential behavior observed experimentally with two configuration classes, combining DFT estimates and relative topological dimerization requirements between PCBM molecules. Excluding sites 1−3 adjacent to the tail, we hypothesize that two populations comprise sites around the equatorial plane (most favorable energetically) and those near the antipode of the tail. It is thus likely that the activation energy assigned to PCBM dimer thermal decomposition, previously estimated as 0.96 eV,[18] is a weighted average $\langle E_a \rangle$ of the site distribution revealed in the present work. Given the DFT energy range computed as approximately $\Delta E_a \simeq 0.10$ eV and our experimental decay rates, we estimate that the two populations exhibit $E_{a,slow} \simeq 0.9$ eV and $E_{a,fast} \simeq 1$ eV, compatible with our observations.

To determine the dominating factor of bond stability the variation of binding energies between classes (i.e., β_a:β_b = 4:4, 4:5, 4:6, etc.) is compared to the variation of binding energies between the same class, but at different orientations (i.e., β_a:β_b = 4_1:4_1, 4_1:4_2, 4_1:4_3, etc.). The most stable class, β = 4, has greater variability still as two bonds are perpendicular and two parallel, with respect to the PCBM tail. Six configurations of β_A:β_B = 4:4 dimers are simulated in Figure S8. The binding energies of these are highlighted in the histogram in Figure 6c and given in Table S1. Although the dimers are topologically very different, the effect on binding energy is less significant. This is not unexpected as changing the bonding orientation might have little effect on the strain experienced by the cage. From these results the dimer bonding position relative to the PCBM tail, β, is the dominant factor in determining the binding energy of the dimer. In addition, the formation energy of dimer 8:8 was calculated to be +28 meV, which is less stable than the dimer formation set to a reference value of zero. This can be explained considering that, on the one hand, two new bonds are created, but on the other hand some of the fullerene aromaticity is lost, and since these are antagonist effects, it explains the positive energy of formation required. To gain insight into this apparent anomaly, aromaticity analysis was performed. The NICS(0) indexes of the rings involved in the bond creations became strongly antiaromatic. In detail, from values of −2.90 and −2.97 for a single PCBM to values of +3.77 and 5.96 for position 8 (negative values mean aromaticity, positive antiaromaticity). This aromaticity lost sheds light into the positive formation energy obtained for position 8:8.

Finally, to understand the effect of PCBM dimer configuration on device performance the variations on frontier molecular orbitals (FMO) are considered. Figure 7 reports the HOMO and the LUMO energy values compared to the dimer binding energy of formation. The HOMO and LUMO energies of the PCBM molecule calculated with these simulation conditions, at −5.57 eV and −3.00 eV, respectively, are considered as a reference. The lines are least-squares error fits to the data. As for the previous analysis, a strong correlation is obtained between the bonds formation energy and the FMO energy. A stabilization of the HOMO and LUMO with greater dimer binding energy was found. This is directly related to the fact that the higher the stability of a molecule, the deeper the

DOI: 10.1021/acs.chemmater.8b05194
Chem. Mater. 2019, 31, 6076−6083

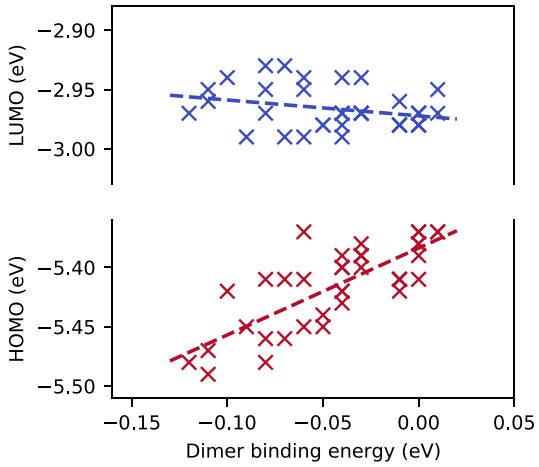

Figure 7. Effect of PCBM dimerization on the frontier molecular orbital levels as calculated by DFT simulations. The stabilization of the dimer binding energy results in the widening of the band gap. Dimerization results in the increased disorder of both the HOMO and the LUMO level. The solid lines present fits with the least-squares error.

electronic levels of the HOMO, which corresponds to a gain in electronic energy. From these results, it is concluded that the dimer binding energy will affect the electronic properties of PCBM.

4. DISCUSSION

Previous studies have shown PCBM dimerization to be correlated with both beneficial and detrimental effects on stability. Typically, studies presenting the preferential effect of PCBM dimerization are performed at low light irradiance (≈0.1 Sun). However, studies demonstrating the degradation induced by dimerization are performed at higher light irradiance (≈1 Sun). Here it is shown that the irradiance affects the formation of the dimer configuration and, subsequently, the molecular orbital levels. At high light intensities, a larger proportion of strongly bound dimers are formed. These dimers are calculated to have a LUMO level 2−3 kT greater than that of PCBM and as such effect the mobility of polarons through PCBM. At lower light intensities greater weakly bound dimers are formed which have a LUMO approximately equal to the PCBM monomer. With this understanding, it is possible to comprehend the double-edged effects of dimerization.

The photophysics and irradiance dependence of the dimerization reaction has been reported as a mono-excited mechanism in C_{60} by Eklund and co-workers[22] and bi-excited mechanism in PCBM by Edman and co-workers.[32] Here, we investigate the irradiance and radiant exposure of PCBM dimerization as a mechanism to probe the effect on the formation of strong and weak dimers. In Figure 3a, after irradiance varying nearly 2 orders of magnitude, we find the extent of dimerization varies by ±8%. Although these values do not support the biexcited model, it does raise an interesting point regarding the slight irradiance dependence on the extent of dimerization which is likely correlated with dimer configurations reported in this paper.

The formation of the de-dimerization fast- and slow-phases have different photophysical mechanisms. The fast phase of weakly bound dimers was time-dependent while the slow phase of strongly bound dimers was irradiance dependent. This is likely due to the matrix constraining the orientation of the weak dimers such that the correct alignment occurs infrequently. Interpreting the formation of strong and weak dimers with these mechanisms allows for the comprehension of the irradiance dependence of dimerization. At higher irradiance, dimers are saturated in the strong configuration before weak dimers are formed, while at lower irradiance, dimers are able to form in both weak and strong configurations. The different factors limiting the weak and the strong dimerization results in an irradiance dependence of formation.

The dominant PCBM dimerization mechanism during the operation of a solar cell will be greatly affected by the location. To predict the overall beneficial or detrimental effects of dimerization it is important to consider the diurnal and annual irradiance variation. A solar cell is likely to exhibit the greatest thermal stress while at high light intensities. The beneficial effects of morphological stability under thermal stress will only be experienced under high light intensity resulting in strongly bound dimers. Additionally, the cyclic conditions will result in the equilibrium tending toward the most stable strongly bound dimer. Therefore, under operating conditions of a solar cell it may be unavoidable not to form the detrimental strongly bound dimers that have been associated with “burn-in”.

5. CONCLUSIONS

This work rationalizes the reasons for the double-edged effects of PCBM dimerization previously reported in the literature. By investing the de-dimerization kinetics upon thermal annealing two populations of dimers have been found to form. Photodimerization at high irradiance is shown to result in strongly bound dimers, while at lower irradiance weakly bound dimers are also formed. DFT calculations suggest the origin of this energetic distribution in dimer binding energy originates in the location of the PCBM tail with respect to the dimer bonds on the fullerene cage. The simulations also show the dimer binding energy is correlated with molecular orbital levels. The ideas presented enable a pathway to comprehend the varied effects of PCBM dimerization on device stability.

■ ASSOCIATED CONTENT

Supporting Information

The Supporting Information is available free of charge on the ACS Publications website at DOI: 10.1021/acs.chemmater.8b05194.

Details on the LED spectrum, dimerization calibration, bi-exponential fitting, stong/weak dimer irradiance dependence, dimer bonding locations, DFT calculations of dimer strain, and additional DFT simulations on PCBM dimer configurations (PDF)

■ AUTHOR INFORMATION

Corresponding Authors

*(J.T.C.) E-mail: j.cabral@imperial.ac.uk.
*(J.R.D.) E-mail: j.durrant@imperial.ac.uk.

ORCID

Sebastian Pont: 0000-0002-0087-9989
Silvio Osella: 0000-0001-8541-1914
Zhe Li: 0000-0003-1149-7000
David Beljonne: 0000-0002-2989-3557
João T. Cabral: 0000-0002-2590-225X

DOI: 10.1021/acs.chemmater.8b05194
Chem. Mater. 2019, 31, 6076−6083

James R. Durrant: 0000-0001-8353-7345

Notes

The authors declare no competing financial interest.
Data presented in this paper is available on request.

■ ACKNOWLEDGMENTS

We would like thank the Engineering and Physical Sciences Research Council (EPSRC, UK, EP/L016702/1) and Solvay for financial support. Z.L. thanks the Welsh Assembly Government Ser Cymru II fellowship scheme for financial support.

■ REFERENCES

(1) Gevorgyan, S. A.; Madsen, M. V.; Roth, B.; Corazza, M.; Hösel, M.; Søndergaard, R. R.; Jørgensen, M.; Krebs, F. C. Lifetime of Organic Photovoltaics: Status and Predictions. *Adv. Energy Mater.* **2016**, *6* (1), 1501208.
(2) Zhao, J.; Li, Y.; Yang, G.; Jiang, K.; Lin, H.; Ade, H.; Ma, W.; Yan, H. Efficient organic solar cells processed from hydrocarbon solvents. *Nature Energy* **2016**, *1* (1), 15027.
(3) Zhang, S.; Ye, L.; Hou, J. Breaking the 10% Efficiency Barrier in Organic Photovoltaics: Morphology and Device Optimization of Well-Known PBDTTT Polymers. *Adv. Energy Mater.* **2016**, *6* (11), 1502529.
(4) Zhao, W.; Li, S.; Yao, H.; Zhang, S.; Zhang, Y.; Yang, B.; Hou, J. Molecular Optimization Enables over 13% Efficiency in Organic Solar Cells. *J. Am. Chem. Soc.* **2017**, *139* (5), 7148−7151.
(5) Meng, L.; Zhang, Y.; Wan, X.; Li, C.; Zhang, X.; Wang, Y.; Ke, X.; Xiao, Z.; Ding, L.; Xia, R.; Yip, H.-L.; Cao, Y.; Chen, Y. Organic and solution-processed tandem solar cells with 17.3% efficiency. *Science* **2018**, *361* (9), 1094−1098.
(6) Lee, H. K. H.; Telford, A. M.; Röhr, J. A.; Wyatt, M. F.; Rice, B.; Wu, J.; de Castro Maciel, A.; Tuladhar, S. M.; Speller, E.; McGettrick, J.; Searle, J. R.; Pont, S.; Watson, T.; Kirchartz, T.; Durrant, J. R.; Tsoi, W. C.; Nelson, J.; Li, Z. The role of fullerenes in the environmental stability of polymer:fullerene solar cells. *Energy Environ. Sci.* **2018**, *11* (2), 417−428.
(7) Mateker, W. R.; McGehee, M. D. Progress in Understanding Degradation Mechanisms and Improving Stability in Organic Photovoltaics. *Adv. Mater.* **2017**, *29* (3), 1603940.
(8) Fraga Domínguez, I.; Distler, A.; Lüer, L. Stability of Organic Solar Cells: The Influence of Nanostructured Carbon Materials. *Adv. Energy Mater.* **2017**, *7* (5), 1601320.
(9) Jørgensen, M.; Norrman, K.; Gevorgyan, S. A.; Tromholt, T.; Andreasen, B.; Krebs, F. C. Stability of Polymer Solar Cells. *Adv. Mater.* **2012**, *24* (2), 580−612.
(10) Savagatrup, S.; Printz, A. D.; O'Connor, T. F.; Zaretski, A. V.; Rodriquez, D.; Sawyer, E. J.; Rajan, K. M.; Acosta, R. I.; Root, S. E.; Lipomi, D. J. Mechanical degradation and stability of organic solar cells: molecular and microstructural determinants. *Energy Environ. Sci.* **2015**, *8* (1), 55−80.
(11) Cheng, P.; Yan, C.; Wu, Y.; Wang, J.; Qin, M.; An, Q.; Cao, J.; Huo, L.; Zhang, F.; Ding, L.; Sun, Y.; Ma, W.; Zhan, X. Alloy Acceptor: Superior Alternative to PCBM toward Efficient and Stable Organic Solar Cells. *Adv. Mater.* **2016**, *28* (36), 8021−8028.
(12) Chen, W.; Nikiforov, M. P.; Darling, S. B. Morphology characterization in organic and hybrid solar cells. *Energy Environ. Sci.* **2012**, *5* (7), 8045.
(13) Kang, H.; Lee, W.; Oh, J.; Kim, T.; Lee, C.; Kim, B. J. From Fullerene-Polymer to All-Polymer Solar Cells: The Importance of Molecular Packing, Orientation, and Morphology Control. *Acc. Chem. Res.* **2016**, *49* (11), 2424−2434.
(14) Guerrero, A.; Garcia-Belmonte, G. Recent Advances to Understand Morphology Stability of Organic Photovoltaics. *Nano-Micro Letters* **2017**, *9* (1), 10.
(15) Distler, A.; Sauermann, T.; Egelhaaf, H.-J.; Rodman, S.; Waller, D.; Cheon, K.-S.; Lee, M.; Guldi, D. M. The Effect of PCBM Dimerization on the Performance of Bulk Heterojunction Solar Cells. *Adv. Energy Mater.* **2014**, *4* (1), 1300693.
(16) Heumueller, T.; Mateker, W. R.; Distler, A.; Fritze, U. F.; Cheacharoen, R.; Nguyen, W. H.; Biele, M.; Salvador, M.; von Delius, M.; Egelhaaf, H.-J.; McGehee, M. D.; Brabec, C. J. Morphological and electrical control of fullerene dimerization determines organic photovoltaic stability. *Energy Environ. Sci.* **2016**, *9* (1), 247−256.
(17) Li, Z.; Wong, H. C.; Huang, Z.; Zhong, H.; Tan, C. H.; Tsoi, W. C.; Kim, J. S.; Durrant, J. R.; Cabral, J. T. Performance enhancement of fullerene-based solar cells by light processing. *Nat. Commun.* **2013**, *4* (1), 2227.
(18) Wong, H. C.; Li, Z.; Tan, C. H.; Zhong, H.; Huang, Z.; Bronstein, H.; McCulloch, I.; Cabral, J. T.; Durrant, J. R. Morphological Stability and Performance of Polymer-Fullerene Solar Cells under Thermal Stress: The Impact of Photoinduced PC 60 BM Oligomerization. *ACS Nano* **2014**, *8* (2), 1297−1308.
(19) Pont, S.; Foglia, F.; Higgins, A. M.; Durrant, J. R.; Cabral, J. T. Stability of Polymer:PCBM Thin Films under Competitive Illumination and Thermal Stress. *Adv. Funct. Mater.* **2018**, *28* (10), 1802520.
(20) Inasaridze, L. N.; Shames, A. I.; Martynov, I. V.; Li, B.; Mumyatov, A. V.; Susarova, D. K.; Katz, E. A.; Troshin, P. A. Light-induced generation of free radicals by fullerene derivatives: an important degradation pathway in organic photovoltaics? *J. Mater. Chem. A* **2017**, *5* (17), 8044−8050.
(21) Rao, A.; Wang, K.-A.; Holden, J.; Wang, Y.; Zhou, P.; Eklund, P.; Eloi, C.; Robertson, J. Photoassisted oxygen doping of C60 films. *J. Mater. Res.* **1993**, *8* (9), 2277−2281.
(22) Wang, Y.; Holden, J.; Dong, Z.-H.; Bi, X.-X.; Eklund, P. Photo-dimerization kinetics in solid C60 films. *Chem. Phys. Lett.* **1993**, *211*, 341−345.
(23) Dzwilewski, A.; Wågberg, T.; Edman, L. Photo-induced and resist-free imprint patterning of fullerene materials for use in functional electronics. *J. Am. Chem. Soc.* **2009**, *131* (11), 4006−4011.
(24) Distler, A. The Role of Fullerenes in the Photo-degradation of Organic Solar Cells (Die Rolle von Fullerenen bei der Photo-degradation organischer Solarzellen). Ph.D. thesis, University of Erlangen-Nuremberg, 2015.
(25) Keiderling, C.; Dimitrov, S.; Durrant, J. R. Exciton and Charge Generation in PC 60 BM Thin Films. *J. Phys. Chem. C* **2017**, *121* (7), 14470−14475.
(26) Wang, Y.; Holden, J.; Bi, X. X.; Eklund, P. Thermal decomposition of polymeric C60. *Chem. Phys. Lett.* **1994**, *217* (1), 413−417.
(27) Eklund, P.; Rao, A.; Zhou, P.; Wang, Y.; Holden, J. Photochemical transformation of C60 and C70 films. *Thin Solid Films* **1995**, *257* (3), 185−203.
(28) Pont, S.; Durrant, J. R.; Cabral, J. T. Dynamic PCBM:Dimer Population in Solar Cells under Light and Temperature Fluctuations. *Adv. Energy Mater.* **2019**, *3*, 1803948.
(29) Stepanian, S. G.; Karachevtsev, V. A.; Plokhotnichenko, A. M.; Adamowicz, L.; Rao, A. M. IR Spectra of Photopolymerized C 60 Films. Experimental and Density Functional Theory Study. *J. Phys. Chem. B* **2006**, *110* (8), 15769−15775.
(30) Adams, G. B.; Page, J. B.; Sankey, O. F.; O'Keeffe, M. Polymerized C60 studied by first-principles molecular dynamics. *Phys. Rev. B: Condens. Matter Mater. Phys.* **1994**, *50* (12), 17471−17479.
(31) Suzuki, M.; Iida, T.; Nasu, K. Relaxation of exciton and photoinduced dimerization in crystalline C60. *Phys. Rev. B: Condens. Matter Mater. Phys.* **2000**, *61* (1), 2188−2198.
(32) Wang, J.; Enevold, J.; Edman, L. Photochemical Transformation of Fullerenes. *Adv. Funct. Mater.* **2013**, *23* (7), 3220−3225.

DOI: 10.1021/acs.chemmater.8b05194
Chem. Mater. 2019, 31, 6076−6083